Inorg. Chem. **2006**, *45*, 4580–4582

Channel-Switching Crystal with Guest Stress Drive

Satoshi Takamizawa,* Kenichi Kojima, and Takamasa Akatsuka

International Graduate School of Arts and Sciences, Yokohama City University, Kanazawa-ku, Yokohama, Kanagawa 236-0027, Japan

Received November 11, 2005

By the addition of a "leverage" mechanism in a host component of a metal–organic crystal, a channel-switching property was developed in a porous single-crystal adsorbent driven by incorporated guest gas stress, which may provide new single-crystal devices with the active controllability of anisotropic guest diffusivity.

Although the recent development of a method of construction for achieving porosity has produced various designable porous solids in metal−organic[1] and organic materials[2] and focused on dynamic porosity and diffusion of gaseous guests inside,[2−5] the observable bulk property is usually unrelated to the crystal anisotropy because of their microcrystalline or powder states. Because the gas adsorption phenomena based on porosity can be applied to a wide range of utilizations such as gas purification, storage, and catalysts, sufficiently sized porous single solids bearing changeable structures can implement advanced applications by using gas anisotropic diffusivity and active modulation of porosity. However, there is an inevitable conflict in investing a porous substance with both the properties of stability of single-crystal morphology and an increase in its structural changeability. Here, we report on our success in achieving a new class of dynamic porosity by adding a degree of freedom to the host skeleton as a mechanism of "molecular leverage". This mechanism can actively switch the inner channel topology by maintaining the single-crystal morphology triggered by the incorporated guest gas stress.

Scheme 1. Schematic Drawing of Channel Transformation by Guest Stress[a]

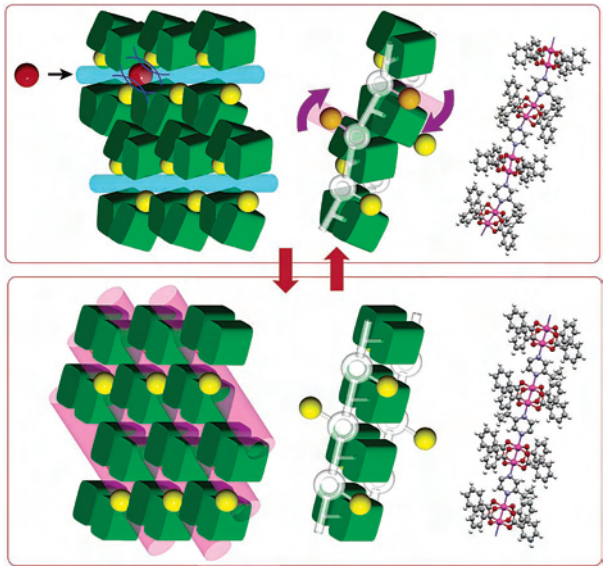

[a] The red and yellow balls indicate the adsorbed guest inside the crystal, and the green cubes show the phenyl rings of the benzoate ligands. The channels are depicted as blue and red pipes [packing change (left), springlike chain motion by leverage (middle), and a real ball-and-stick model of rhodium(II) benzoate 2-ethylpyrazine chain complex (**1**) (right)].

We have previously reported on the metal−organic single-crystal porous solid $[M^{II}(bza)_4(pyz)]_n$ (M = Rh and Cu; bza = benzoate; pyz = pyrazine).[6] To introduce the "lever" into a porous single crystal, an ethyl-substituted derivative of $[Rh^{II}_2(bza)_4(2\text{-epyz})]_n$ (**1**) (2-epyz = 2-ethylpyrazine) was prepared.[7] The obtained single crystal was formed by the assembly of an infinite zigzag 1-D coordination polymer chain through only weak intermolecular interaction of phenyl−pyrazine and quadruple phenyl−phenyl stacking,

* To whom correspondence should be addressed. E-mail: staka@yokohama-cu.ac.jp.

(1) (a) Yaghi, O. M.; O'Keeffe, M.; Ockwig, N. W.; Chae, H. K.; Eddaoudi, M.; Kim, J. *Nature* **2003**, *423*, 705. (b) Kitagawa, S.; Kitaura, R.; Noro, S.-i. *Angew. Chem., Int. Ed.* **2004**, *43*, 2334. (c) Mori, W.; Takamizawa, S. In *Organometallic Conjugation—Structures, Reactions and Functions of d−d and d−π Conjugated Systems*; Nakamura, A., Ueyama, N., Yamaguchi, K., Eds.; Springer-Verlag: Berlin, 2002; Chapter 6.

(2) Atwood, J. L.; Barbour, L. J.; Jerga, A.; Schottel, B. L. *Science* **2002**, *298*, 1000.

(3) (a) Biradha, K.; Hongo, Y.; Fujita, M. *Angew. Chem., Int. Ed.* **2002**, *41*, 3395. (b) Cussen, E. J.; Claridge, J. B.; Rosseinsky, M. J.; Kepert, C. J. *J. Am. Chem. Soc.* **2002**, *124*, 9574. (c) Matsuda, R.; Kitaura, R.; Kitagawa, S.; Kubota, Y.; Kobayashi, T.-C.; Horike, S.; Takata, M. *J. Am. Chem. Soc.* **2004**, *126*, 14063.

(4) (a) Atwood, J. L.; Barbour, L. J.; Jerga, A. *Angew. Chem., Int. Ed.* **2004**, *43*, 2948. (b) Sozzani, P.; Comotti, A.; Bracco, S.; Simonutti, R. *Angew. Chem., Int. Ed.* **2004**, *43*, 2792.

(5) (a) Takamizawa, S.; Nakata, E.; Yokoyama, H.; Mochizuki, K.; Mori, W. *Angew. Chem., Int. Ed.* **2003**, *42*, 4331. (b) Takamizawa, S.; Nakata, E.; Saito, T. *Inorg. Chem. Commun.* **2004**, *7* (1), 1. (c) Takamizawa, S.; Nakata, E.; Saito, T. *CrystEngComm* **2004**, *6* (9), 39.

(6) (a) Takamizawa, S.; Hiroki, T.; Nakata, E.; Mochizuki, K.; Mori, W. *Chem. Lett.* **2002**, *2002*, 1208. (b) Takamizawa, S.; Nakata, E.; Yokoyama, H. *Inorg. Chem. Commun.* **2003**, *6*, 763.

(7) $[Rh_2(bza)_4(2\text{-epyz})]_n$ (**1**) was synthesized by a method similar to that for the pyrazine derivative reported in ref 6a, which obtained as red plates in 60.7% yield. Calcd for $C_{34}H_{28}N_2O_8Rh_2$: C, 51.15; H, 3.53; N, 3.51. Found: C, 50.95; H, 3.41; N, 3.69.

10.1021/ic051952e CCC: $33.50
Published on Web 04/29/2006

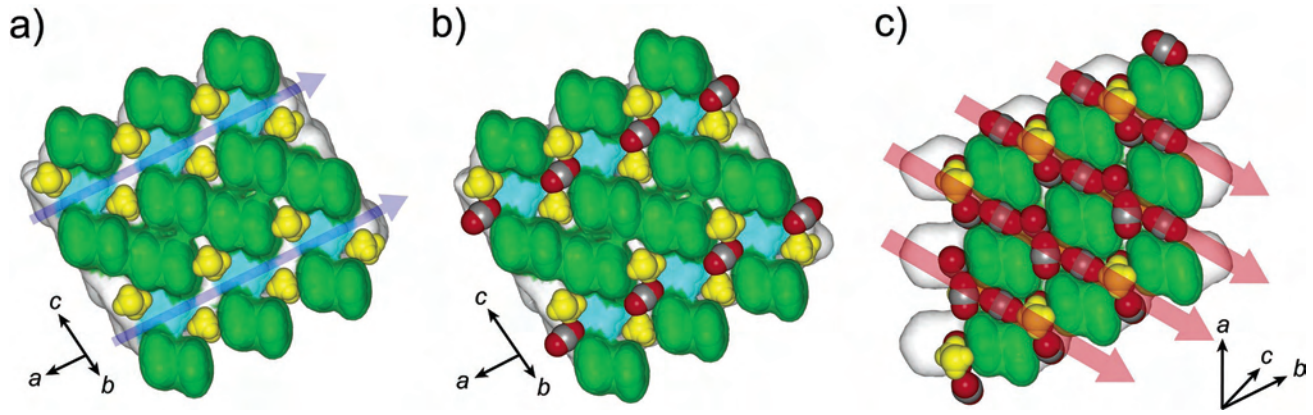

Figure 1. Intersection views of single crystal **1** under various conditions: α-**1** without gas at 298 K (a); CO_2-adsorbed states of **1** with α-**1**$(CO_2)_{0.075}$ composition (CO_2 site occupancy is 0.15) at 298 K at 6.4 MPa gas pressure (b); with β-**1**·3CO_2 composition at 90 K (3.6 MPa at room temperature) (c). These intersection views are along the crystal morphology as shown in Figure 3. Guest (CO_2)−host (ethyl group) contact in α-**1** (b) generates a stressed structure, inducing the channel structural transformation to β-**1**. Included CO_2 molecules and ethyl moieties are depicted using a ball-and-stick model. Yellow indicates ethyl groups on the channel surface; green and blue indicate $\pi-\pi$ stacking benzene rings, respectively. The blue and green arrows in parts a and c indicate the directions of 1-D channels in the α and β phases of **1**, respectively (see the main text).

where the chain skeleton was bent by the steric hindrance of the ethyl group on a pyrazine linker against a dinuclear rhodium benzoate core[8−10] (Scheme 1 and Figure 1a). The crystal **1** has small vacant cavities of 35(1) Å^3 in volume[11] sandwiched by the ethyl groups exposed on the cavity (Figure 1a,b), which demonstrates that the substitution of the host skeleton can modify the inner surface by molecular design.

Although the nonpenetrated porous structure was obstructed by stacking phenyl rings (colored blue and green in Figure 1), the CO_2 gas adsorption property (Figure 2) demonstrated the existence of a dynamic guest diffusive pathway among the vacant cavities. From the structural difference in obstructing phenyl−phenyl stacking, the sites colored blue are loosely stacked whereas the sites colored green are tight, which indicates that the guest incorporated inside the crystal can diffuse through the stacked blue-colored benzene rings, which can be regarded as a dynamic 1-D channel diffusion.[12]

The crystal **1** can absorb a large amount of gas involving a α−β bulk phase transition with a critical amount of gas adsorbed. The CO_2 gas sorption isotherm indicates the

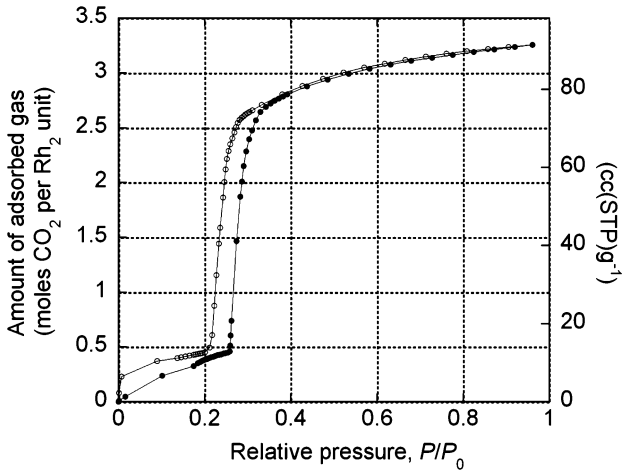

Figure 2. Cyclic CO_2 sorption isotherm curve at 195 K for single crystals of **1**. [The unit of cc(STP) means the amount of adsorbed gas by volume under standard conditions (0 °C, 0.1 MPa).]

smooth reversibility of **1** with slight hysteresis in the sorption leap region around a relative pressure of 0.3 at 195 K[13] (Figure 2). The adsorption leap occurs at an adsorption amount of 0.5 CO_2 molecule per Rh_2 unit, which indicates that the beginning point of the α−β phase transition of **1** can be regarded as the α-saturated state where all cavities are stoichiometrically occupied by the incorporated gas molecules. Furthermore, the sorption behavior before and after the adsorption leap demonstrates the smooth diffusion

(8) All single-crystal X-ray analyses were performed on a Bruker Smart APEX CCD area diffractometer with a nitrogen-flow temperature controller using graphite-monochromated Mo Kα radiation (λ = 0.710 73 Å). A single crystal of **1** was sealed in a glass capillary containing solid CO_2 in a liquid-nitrogen bath. The inner pressure at room temperature was estimated by the ratio of the volumes of condensed gas and inner space. Empirical absorption corrections were applied using the *SADABS* program. The structures were solved by direct methods (*SHELXS-97*) and refined by full-matrix least-squares calculations on F^2 (*SHELXL-97*) using the *SHELX-TL* program package. CCDC-280024-280027.

(9) Crystal data for **1** at 298 K: 798.40 g mol^{-1}, triclinic, $P\bar{1}$, a = 10.5184(7) Å, b = 10.5191(8) Å, c = 15.6108(11) Å, α = 81.007°, β = 79.760°, γ = 87.933°, V = 1678.8(2) Å^3, Z = 2, d_{calcd} = 1.579 Mg m^{-3}, R1 = 0.0507 (0.0819), wR2 = 0.1069 (0.1394) for 4182 reflections with $I > 2\sigma(I)$ [for 5930 reflections (9908 total measured)], GOF on F^2 = 1.093, largest diffraction peak (hole) = 0.828 (−0.900) e Å^{-3}.

(10) Crystal data for **1** at 90 K: 798.40 g mol^{-1}, triclinic, $P\bar{1}$, a = 10.2833(10) Å, b = 10.4707(10) Å, c = 15.5700(15) Å, α = 79.133(2)°, β = 81.323(2)°, γ = 86.287(2)°, V = 1626.4(3) Å^3, Z = 2, d_{calcd} = 1.630 Mg m^{-3}, R1 = 0.0510 (0.0742), wR2 = 0.1058 (0.1281) for 4352 reflections with $I > 2\sigma(I)$ [for 5739 reflections (9565 total measured)], GOF on F^2 = 1.067, largest diffraction peak (hole) = 0.896 (−1.024) e Å^{-3}.

(11) The discrete void volume was calculated by using probe radii: C (1.70 Å), H (1.20 Å), N (1.55 Å), O (1.52 Å), and Rh (2.25 Å).

(12) The structural difference in the temperature and surrounding gas condition shows a lesser dependency of the phenyl−phenyl distance for the blue color sites in maintaining 3.50−3.60 Å, while those of the center stacking of the green color sites was 3.35−3.47 Å and the offset distance is more changeable in the blue stacking rings in 3.23−3.72 Å than that of the green color rings in 3.02−3.40 Å (see Figure 1 and Table S5 in the Supporting Information). This strongly indicates that the blue-colored stacking sites are loose and independent of the support for the crystal packing. Thus, there is a greater possibility that blue color stacking can dynamically open to allow the gas molecules to diffuse inside the crystal (see the Supporting Information).

(13) The CO_2 adsorption isotherm was measured on a Quantachrome Autosorb-1 at 195 K under a relative pressure (P/P_0, where P_0 = saturation vapor pressure) range from 10^{-2} to 1.

of the incorporated gas molecules within both channels in the α and β phases (Figure 2). The gas adsorption dependency of the bulk phase transition of **1** was observed in differential scanning calorimetry (DSC) measurements at various partial pressures of CO_2 (see the Supporting Information), which revealed that this bulk phase transition, categorized as "mass-induced phase transition",[14] is strongly correlated with gas adsorption phenomena. Consequently, this phase transition can be regulated by control of thermodynamic factors such as the temperature, pressure, and gas concentration of various gaseous guests. Interestingly, DSC measurements revealed the large enthalpy of the bulk phase transition of **1** (ΔH = 39.1 kJ mol^{-1}) with the small adsorption enthalpy of the guest CO_2 gas (ΔH_{iso} = 37.9 kJ mol^{-1}) (see the Supporting Information). This strongly suggests the efficient driving mechanism in **1** for the transformation, which can employ large structural changes smoothly and reversibly by the phenomenon of weak gas physisorption.

Characterization of the host structural change during the phase transition was captured by single-crystal X-ray diffraction analysis under a CO_2 gas atmosphere.[15,16] Determination of the CO_2 adsorption state in the α phase of **1** before the phase transition was performed at room temperature, demonstrating the anticipated structure wherein CO_2 molecules are included in the small cavities in contact with the ethyl moieties on the channel surface (Figure 1b). Alternatively, the β-phase structure of **1** after the phase transition was successfully caught at 90 K (Figure 1c). The structure of the inner space changed dramatically after the phase transition. The switching of the channel direction and an increase in the number of running channels were achieved from the springlike stretching motion of the 1-D polymer chain skeleton (Figures 1 and 3). The bending angle changes from 166° to 180°, accompanying the division of quadruple-stacking benzene rings into double-stacking ones to enable the change of channel topology (refer to Scheme 1). While the amount of void space in the crystal expanded considerably from 2.0% to 12.4% of the crystal volume during α−β transformation, the crystal volume expanded by almost the same degree, 10.9%. This indicates that the efficient transformation of **1** plays an important role in maintaining a single solid state by suppressing crystal distortion.

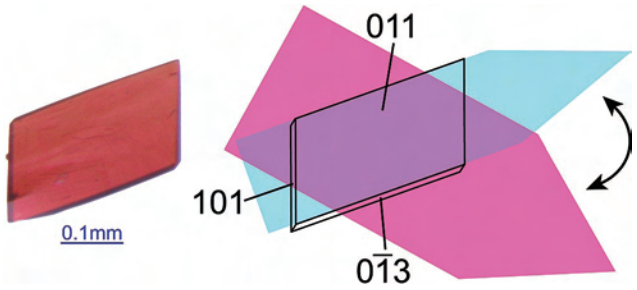

Figure 3. Photograph of single crystal **1** (left) and phase indexing from the crystal structure of α-**1** at 298 K with colored arrows to indicate the channel direction in the α (blue) to β (pink) phases of **1** (right). The directions of the crystals are located along the crystal structures depicted in Figure 1.

From single-crystal X-ray structures for CO_2 gas adsorption states in the α and β phases, the incorporated gas molecules destabilize the α-phase crystal lattice by acting as a stress on the ethyl groups, which initiates a local structural change, leading to the bulk phase transition. This can be considered a "molecular leverage mechanism", where the pushing force of the incorporated guest concentrated on the ethyl moieties (the point of force) forces the bent M−pyrazine−N linking (the point of application) to stretch into the straight 1-D skeleton. The fulcrum force is generated by the reaction of the packing force to position the 1-D chain skeleton at a fixed location in the crystal.

In conclusion, a channel-switching single crystal, which can drastically change pore topology in maintaining single-solid morphology, was synthesized by the addition of a degree of freedom to the host crystal component by molecular design of the host component. The applied mechanical drive can cooperatively increase the local structural change up to the entire range of the crystal. Designable dynamic porous single-solid devices may generate new applications by the active controllability of anisotropic guest diffusivity based on sorption and diffusion phenomena.

Acknowledgment. This work was financially supported by the Ministry of Education, Culture, Sports, Science and Technology, Japan (Grants 16750051 and 17036056), 2005 Strategic Research Project grant of Yokohama City University (Grant K17025), and the Mitsubishi Chemical Corp. Fund.

Supporting Information Available: Crystallographic data (also in CIF format), ORTEP and packing views, and DSC results (PDF). These materials are available free of charge via the Internet at http://pubs.asc.org.

IC051952E

(14) Takamizawa, S.; Saito, T.; Akatsuka, T.; Nakata, E. *Inorg. Chem.* **2005**, *44* (5), 1421.

(15) Crystal data for **1**·3(CO_2) at 90 K (3.6 MPa at room temperature): 930.43 g mol^{-1}, triclinic, $P\bar{1}$, a = 9.607(3) Å, b = 10.321(3) Å, c = 11.530(4) Å, α = 67.522(6)°, β = 65.428(5)°, γ = 63.319(5)°, V = 901.7(5) Å^3, Z = 1, d_{calcd} = 1.714 Mg m^{-3}, R1 = 0.0885 (0.1681), wR2 = 0.2040 (0.2528) for 2082 reflections with $I > 2\sigma(I)$ [for 3724 reflections (4673 total measured)], GOF on F^2 = 0.984, largest diffration peak (hole) = 3.699 (−2.134) e Å^{-3}.

(16) Crystal data for **1**·$(CO_2)_{0.075}$ at 298 K at a 6.4 MPa CO_2 gas atmosphere: 801.70 g mol^{-1}, triclinic, $P\bar{1}$, a = 10.5231(10) Å, b = 10.5597(11) Å, c = 15.6019(14) Å, α = 81.092(2)°, β = 79.994(2)°, γ = 88.246(2)°, V = 1686.7(3) Å^3, Z = 2, d_{calcd} = 1.579 Mg m^{-3}, R1 = 0.0457 (0.0772), wR2 = 0.0994 (0.1172) for 4144 reflections with $I > 2\sigma(I)$ [for 5961 reflections (9891 total measured)], GOF on F^2 = 1.014, largest diffration peak (hole) = 1.340 (−0.571) e Å^{-3}.